24th INTERNATIONAL CONGRESS ON SOUND AND VIBRATION
23–27 July 2017, London

ICSV24
23-27JULY 2017
LONDON CALLING

THE INFLUENCE OF THE KERF WIDTH OF A PLANAR ARRAY ON THE TRANSCRANIAL FOCUSED ULTRASOUND FIELD

Xiangda Wang

State Key Laboratory of Acoustics, Institute of Acoustics, Chinese Academy of Sciences, Beijing, 100190, China
University of Chinese Academy of Sciences, Beijing 100049, China
email: wangxiangda1990@163.com

Weijun Lin, Chang Su, and Hanyin Cui

State Key Laboratory of Acoustics, Institute of Acoustics, Chinese Academy of Sciences, Beijing, 100190, China

A 256-element planar phased array has been designed for the transcranial focused ultrasound (tcFUS) stimuli. A planar phased array is usually fabricated by cutting a large piezoelectric ceramic (PZT) plane. The kerf width is the width of the gap between two adjacent elements, and it may affect the focusing effect. In this paper, the influence of the kerf width of our planar array on the transcranial focused ultrasound field has been studied numerically, in order to assist the design of the array. Seven kerf widths of 0.2, 0.4, 0.45, 0.5, 0.55, 0.6, and 0.8mm are selected, and the target points are located at 40, 50, and 60mm in front of the array centre, respectively. The time reversal method is used to achieve a precise focusing at the chosen focus location. And the Kelvin-Voigt equation is applied to simulate the focusing pressure field of the phased array in water with and without a monkey skull inserted between the phased array and the focus, respectively. Numerical results show that a kerf width smaller than 1/4 wavelength helps to improve the focusing accuracy of the array and that more acoustic energy is focused at the target location as the kerf width becomes smaller. Meanwhile, it is found that the acoustic energy deposited at the focus region generally increases with the increase of the focal length from 40 mm to 60 mm for an arbitrary kerf width, but the increasing trend gradually slows down, which indicates that there may be an optimal focusing location slightly beyond 60 mm in front of the array centre.

Keywords: tcFUS, kerf width, phased array

1. Introduction

Transcranial focused ultrasound (tcFUS) is a rapidly developing technique which is beneficial to the treatments of brain diseases noninvasively [1][2]. Two main obstacles may restrict the clinical applications of the transcranial focused ultrasound technique. One is the overheating of the skull because of the large acoustic impedance difference between the skull and its surrounding tissues and the serious absorption to the acoustic energy by the skull, while the other one is the focal shift caused by the skull's strong inhomogeneity in its acoustic parameters [3]. The development of the ultrasonic phased array transducer since 1990 has provided possibilities to solve these two problems and made the noninvasive transcranial focused ultrasound therapy become possible [4]. For a ultrasonic phased array transducer, the design parameters of the array such as the element spacing, the element distribution and the element size, may have significant influences on the acoustic field radiated by

the array [5][6]. To choose a set of proper design parameters for a phased array transducer is essential for its practical applications on desired occasions.

Recently, a planar ultrasonic phased array transducer with 256 elements and the centre frequency of 0.8MHz has been designed for the transcranial focused ultrasound stimuli in Shenzhen Institutes of Advanced Technology, Chinese Academy of Sciences. This planar phased array is manufactured by regularly cutting a large PZT (piezoelectric ceramic) plane into 16 rows and 16 columns, with a constant element size and a uniform kerf width. The kerf width is the width of the gap between two adjacent elements, and it may affect the transcranial focusing effect of the array. In this paper, the influences of the kerf width of our planar array on the focusing acoustic fields radiated by the array in water with and without the skull inserted between the array and the focusing location have been studied numerically, in order to help the design of the array and to help achieve a good focusing effect. The time reversal method [7] is employed to help the ultrasound to focus at the chosen locations. The computed tomography (CT) scans of a monkey skull are applied for the reconstruction of the three-dimensional skull model and the acquisition of the skull's acoustic parameters [8]. And the Kelvin-Voigt equation [9] with consideration of the mode conversion between compressional waves and shear waves inside the skull solved by staggered-grid finite difference time domain (FDTD) method is adopted for simulations of the acoustic field. Seven kerf widths and three focusing locations are selected for investigations below. And a proper kerf width range for our planar ultrasonic phased array transducer is discussed.

2. Materials and methods

2.1 Planar ultrasonic phased array transducer

The planar ultrasonic phased array transducer to be studied is shown in Fig. 1. A total of 256 elements are regularly distributed in 16 rows and 16 columns with a uniform kerf width. Each element is square with the same size of $3.3\times3.3\text{mm}^2$. The centre frequency of the array is $f_0 = 0.8\text{MHz}$. As for the aim of analysing the influence of the kerf width on the ultrasonic focusing effect by the array, seven kerf widths of 0.2, 0.4, 0.45, 0.5, 0.55, 0.6, and 0.8mm and three focusing locations of 40, 50, and 60mm in front of the array centre are employed for studies.

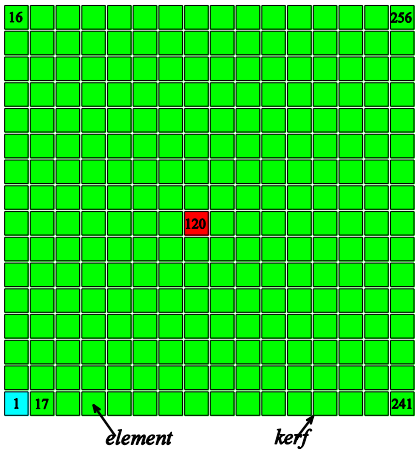

Figure 1: Schematic diagram of the planar ultrasonic phased array transducer

Each element has a uniform emitting acoustic pressure amplitude p_0. For each element of the array, the acoustic pressure radiated is:

$$p_n = p_0 \sin\left(\omega t + \theta_{0n}\right). \tag{1}$$

The subscript n denotes the element number as shown in Fig. 1. The initial emitting phase of the nth element is θ_{0n}.

2.2 Basic equations

To better describe the propagation of ultrasound emitted by the array and account for the mode conversion between compressional waves and shear waves inside the skull, the Kelvin-Voigt equation [9] controlling the ultrasound propagation in the isotropic inhomogeneous viscoelastic media is employed, which can be expressed by the Einstein notation as:

$$\begin{cases} \rho_0 \dfrac{\partial V_i}{\partial t} = \dfrac{\partial T_{ij}}{\partial x_j} \\ \dfrac{\partial T_{ij}}{\partial t} = \lambda \delta_{ij} \dfrac{\partial V_k}{\partial x_k} + \mu \left(\dfrac{\partial V_i}{\partial x_j} + \dfrac{\partial V_j}{\partial x_i} \right) + \chi \delta_{ij} \dfrac{\partial^2 V_k}{\partial x_k \partial t} + \eta \left(\dfrac{\partial^2 V_i}{\partial x_j \partial t} + \dfrac{\partial^2 V_j}{\partial x_i \partial t} \right) \end{cases}. \tag{2}$$

The subscripts i, j and k are Einstein notations. T_{ij} is the stress and V_i is the particle velocity. δ_{ij} is equal to 1 when $i = j$ and is equal to 0 when $i \neq j$. λ and μ are Lame constants, which can be expressed by the density of the media (ρ_0), shear wave velocity (c_s) and compressional wave velocity (c_p) as:

$$\begin{cases} \mu = c_s^2 \rho \\ \lambda + 2\mu = c_p^2 \rho_0 \end{cases}. \tag{3}$$

χ and η are respectively the viscosity coefficients of compressional waves and shear waves, which are related with the compressional wave absorption coefficient (α_p) and the shear wave absorption coefficient (α_s).

$$\begin{cases} \alpha_p \approx \alpha_{0,p} \omega^2 \\ \alpha_s \approx \alpha_{0,s} \omega^2 \end{cases}. \tag{4}$$

$$\begin{cases} \alpha_{0,p} = \dfrac{\chi + 2\eta}{2\rho_0 c_p^3} \\ \alpha_{0,s} = \dfrac{\eta}{2\rho_0 c_s^3} \end{cases}. \tag{5}$$

$\omega = 2\pi f_0$ is the angular frequency. $\alpha_{0,p}$ and $\alpha_{0,s}$ are power law absorption factors.

The staggered-grid finite difference time domain (FDTD) method [10] is adopted to numerically solve the Kelvin-Voigt equation and the perfectly matched layer (PML) [11] absorbing boundary is used to eliminate the reflection of ultrasound at the numerical boundary.

2.3 Reconstruction of 3D skull model

The reconstruction of the three-dimensional (3D) skull model is illustrated in Fig. 2. Generally, CT scans of the skull are utilized to reconstruct the 3D skull model. Here, CT scans of a monkey's skull are provided by Shenzhen Institutes of Advanced Technology, Chinese Academy of Sciences.

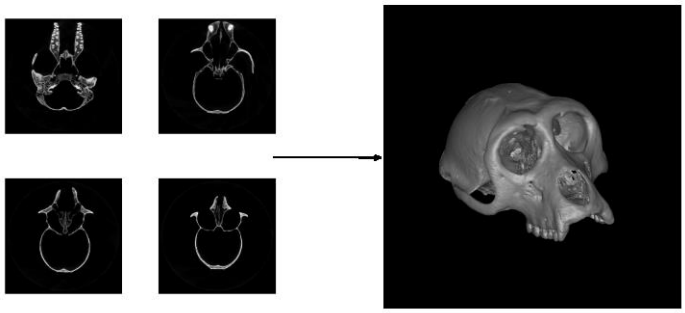

Figure 2: Reconstruction of 3D monkey skull based on CT scans

To obtain the strongly inhomogeneous acoustic parameters of the skull, the relationship between the acoustic parameters and CT values of the skull [8] is applied.

$$\begin{cases} \phi = 1 - \dfrac{H}{1000} \\ \rho = \phi \times \rho_{skull,\min} + (1-\phi) \times \rho_{skull,\max} \\ c_p = \phi \times c_{p,skull,\min} + (1-\phi) \times c_{p,skull,\max} \\ \alpha_p = \alpha_{p,skull,\min} + \phi^{\gamma} \times \left(\alpha_{p,skull,\max} - \alpha_{p,skull,\min} \right) \end{cases} . \tag{6}$$

ρ is the density, c_p is the compressional wave velocity, and α_p is the compressional wave absorption coefficient. H, ϕ, $\rho_{skull,\min}$, $\rho_{skull,\max}$, $c_{p,skull,\min}$, $c_{p,skull,\max}$ and $\alpha_{p,skull,\min}$, $\alpha_{p,skull,\max}$ are the CT value, the porosity, the minimal and maximal densities, the minimal and maximal compressional wave velocities and the minimal and maximal compressional wave absorption coefficients of the skull, respectively. γ is commonly equal to 0.5. The acoustic parameters of the skull used in the simulation are shown in Table 1.

Table 1: Acoustic parameters employed in the simulation [12]

Sound velocity $(\mathrm{m/s})$		Acoustic absorption coefficient $(\mathrm{Np/m})$		Density $(\mathrm{kg/m^3})$	
$c_{p,skull,\min}$	1500	$\alpha_{p,skull,\min}$	7.37	$\rho_{skull,\min}$	1000
$c_{p,skull,\max}$	3100	$\alpha_{p,skull,\max}$	293.12	$\rho_{skull,\max}$	2200
c_{water}	1500	α_{water}	0.000288	ρ_{water}	1000

To calculate the shear wave velocity and the shear wave absorption coefficient of the skull, empirical formulas [12] are generally used, which can be expressed as:

$$\begin{cases} c_s = 4/7 \times c_p \\ \alpha_s = 90/85 \times \alpha_p \end{cases} . \tag{7}$$

where c_s is the shear wave velocity, and α_s is the shear wave absorption coefficient.

2.4 Precise focus control based on time-reversal method

For Eq. (2), according to Eq. (1), the stress conditions for each element become:

$$T_{ij} = -p\,\delta_n . \tag{8}$$

To precisely focus ultrasound excited by the array in water at the chosen target location, especially when there exists a skull, phase modulation is necessary. Here, the time-reversal method is employed to help modulate the initial emitting phase of each element. Ultrasound emitted from a virtual sinusoidal point source $p_{focus} = \sin(\omega t)$ at the focus is recorded by each element of the array. The signal (for example the normal stress T_{xx}) received by an arbitrary element is chosen as reference set as $T_{xx,ref}$ and then undergoes self-correlation and cross-correlations with the received signals of any other elements to help calculate the initial emitting phase θ_{0n} for each element.

3. Numerical results

3.1 Ultrasonic focusing effect of the array dependent on kerf width in pure water

Before analysing the influence of the kerf width of the 256-element planar phased array transducer on the transcranial focused ultrasound field, we first observe the influence of the kerf on the focused ultrasound field in pure water without the skull inserted. The focusing effect of ultrasound emitted

from the array is represented by the acoustic pressure focusing gain (p_f / p_0) where p_f is the acoustic pressure amplitude at the practical focus and the focusing deviation ($\left|\boldsymbol{r}_p - \boldsymbol{r}_t\right|$) between the practical focus location $\boldsymbol{r}_p$ and the theoretical focus location $\boldsymbol{r}_t$. Actually, the acoustic pressure focusing gain denotes the efficiency of the acoustic energy deposited at the focus by the array. In pure water, the acoustic pressure focusing gain and the focusing deviation of the array dependent on the kerf width are respectively shown in Fig. 3 and Fig. 4.

As can be seen from Fig. 3, the acoustic pressure focusing gain decreases with the increase of the kerf width from 0.2mm to 0.8mm for the focal lengths of 50mm and 60mm, indicating a more acoustic energy deposition as the kerf width decreases. However, for the focal length of 40mm, there exists a transition point around 0.5mm and the acoustic pressure focusing gain decreases with the increase of the kerf width from 0.2mm to 0.5mm while then increases with the increase of the kerf width from 0.5mm to 0.8mm, which indicates that the focused ultrasound field is relatively complex when the focus is closer to the array. Additionally, for an arbitrary kerf width studied, the acoustic pressure focusing gain generally increases with the increase of the focal length from 40 mm to 60 mm, but the increasing trend is slowing down, which indicates that there may exist an optimal focal length or focusing location slightly beyond 60mm.

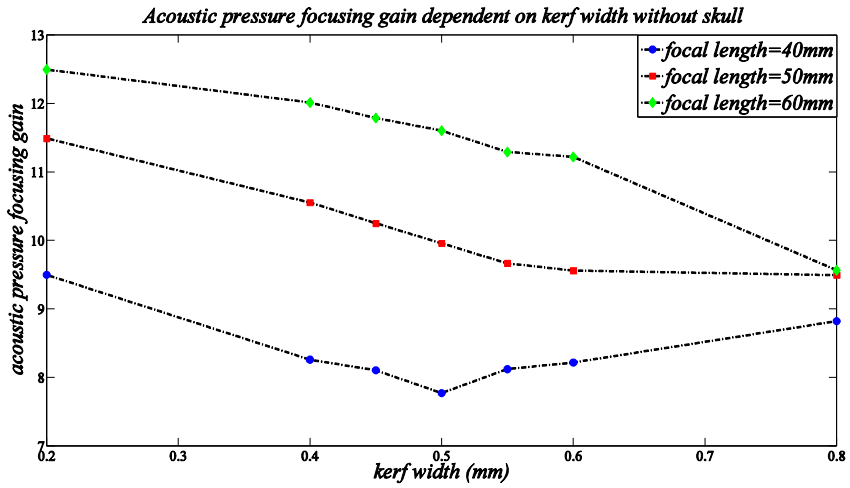

Figure 3: Acoustic pressure focusing gain dependent on kerf width without a skull inserted in water

In Fig. 4, we can see that the focusing deviation basically increases with the increase of the kerf width from 0.2 mm to 0.8 mm for any focal length. Besides, in order to control the focusing deviation lower than 0.5 mm (shown as the red dashed line in Fig. 4) for precise focusing, it is clear that the kerf width is required to be less than 0.5 mm.

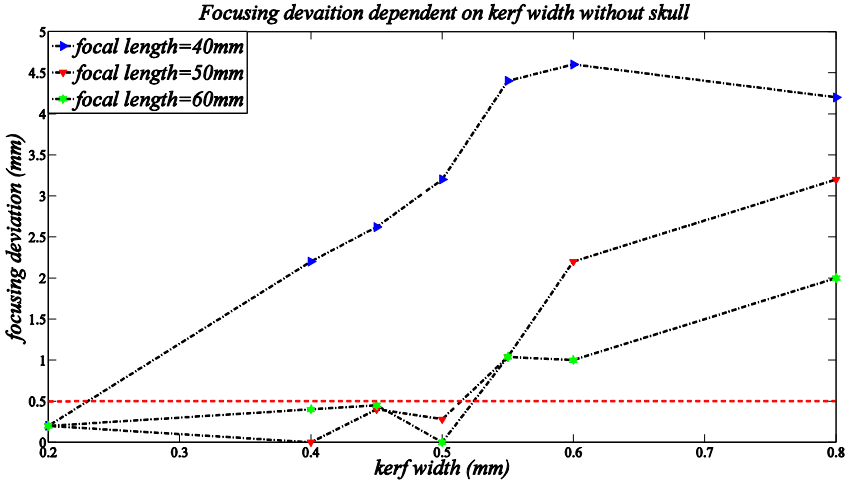

Figure 4: Focusing deviation dependent on kerf width without a skull inserted in water

3.2 Transcranial ultrasonic focusing effect of the array dependent on kerf width

As for the influence of the kerf width of the array on the transcranial focused ultrasound field, the acoustic pressure focusing gain and the focusing deviation introduced in Section 3.1 are also employed here for the analysis of the focusing effect of transcranial ultrasound dependent on the kerf width.

Figure 5 shows the acoustic pressure focusing gain dependent on the kerf width with a skull inserted between the array and the focus in water. The variation tendency of the acoustic pressure focusing gain dependent on the kerf width with a skull is similar to that without a skull in Section 3.1. And, the acoustic pressure focusing gain also increases with the increase of the focal length from 40 mm to 60 mm with the increasing trend slowing down for an arbitrary kerf width, again indicating the existence of an optimal focal length or focusing location slightly beyond 60 mm. However, the acoustic pressure focusing gain with a skull is greatly reduced compared with that without a skull because of the strong scattering and absorption of the skull to ultrasound. Additionally, the transition point for the focal length of 40 mm with a skull is larger than that without a skull.

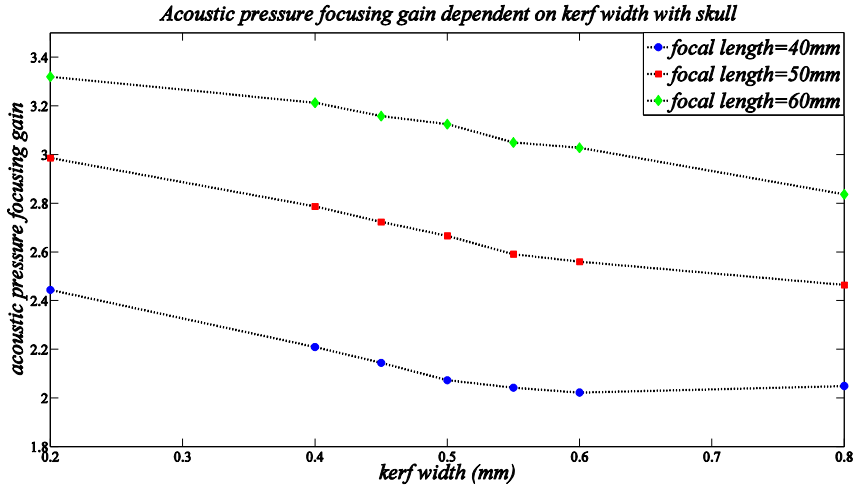

Figure 5: Acoustic pressure focusing gain dependent on kerf width with a skull inserted in water

From Fig. 6 giving the focusing deviation dependent on kerf width with a skull inserted in water, it can be also observed that the variation tendency of the focusing deviation dependent on the kerf width with a skull is basically similar to that without a skull. And, the kerf width required for controlling the focusing deviation lower than 0.5mm (indicated by the red dashed line in Fig. 6) is approximately less than 0.45mm which is nearly 1/4 wavelength for an ultrasound of 0.8MHz in water.

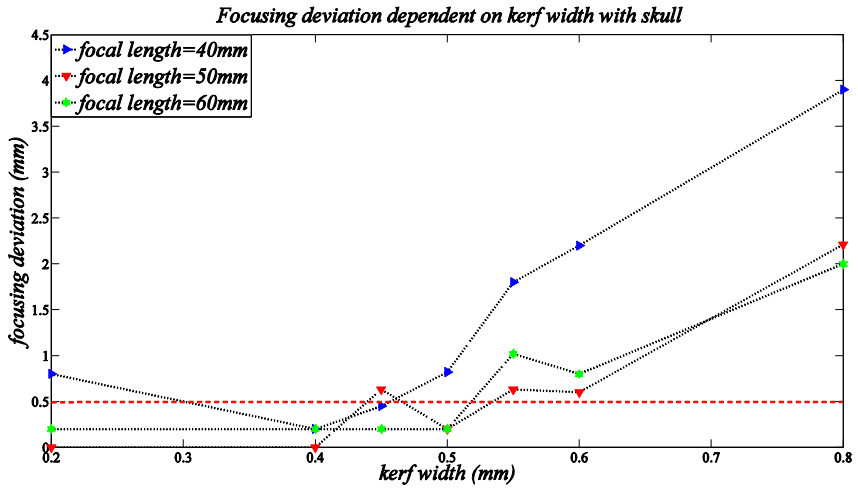

Figure 6: Focusing deviation dependent on kerf width with a skull inserted in water

4. Conclusions

The influence of the kerf width of a 256-element planar phased array transducer on transcranial focused ultrasound is numerically investigated. Seven kerf widths of 0.2, 0.4, 0.45, 0.5, 0.55, 0.6, and 0.8 mm and three target locations of 40, 50, and 60 mm in front of the array centre are combined for studies. For a precise focus control, the time-reversal method is employed. Numerical results of the focused ultrasound fields of the array with and without a monkey skull inserted in water show that a kerf width smaller than 0.45 mm (about 1/4 wavelength for 0.8 MHz ultrasound in water) is beneficial to the improvement of the focusing accuracy of the array and that more acoustic energy can be deposited at the focus location with the decrease of the kerf width. Additionally, it is observed that the acoustic energy deposited at the focus region increases as the focal length increases from 40 mm to 60 mm, while the increasing trend is downward, which indicates that an optimal focusing location slightly beyond 60 mm in front of the array centre may exist.

ACKNOWLEDGEMENTS

This work is supported by the National Natural Science Foundation of China (Grant No. 81527901 and Grant No. 11604361).

REFERENCES

1 Poon, C., McMahon, D., and Hynynen, K. Noninvasive and Targeted Delivery of Therapeutics to the Brain Using Focused Ultrasound, *Neuropharmacology*, (2016).

2 Naor, O., Krupa, S., & Shoham, S. Ultrasonic Neuromodulation, *Journal of Neural Engineering*, 13(3): 031003, (2016).

3 Colen, R. R., & Jolesz, F. A. Future Potential of MRI-guided Focused Ultrasound Brain Surgery, *Neuroimaging Clinics of North America*, 20(3): 355-366, (2010).

4 Kyriakou, A., Neufeld, E., Werner, B., Paulides, M. M., Szekely, G., and Kuster, N. A Review of Numerical and Experimental Compensation Techniques for Skull-induced Phase Aberrations in Transcranial Focused Ultrasound, *International Journal of Hyperthermia*, 30(1): 36-46, (2014).

5 Qi, W., and Cao, W. Finite Element Study on 1-D Array Transducer Design, *IEEE Transactions on Ultrasonics, Ferroelectrics, and Frequency Control*, 47(4): 949-955, (2000).

6 Lee, J. H., and Choi, S. W. A Parametric Study of Ultrasonic Beam Profiles for a Linear Phased Array Transducer, *IEEE Transactions on Ultrasonics, Ferroelectrics, and Frequency Control*, 47(3): 644-650, (2000).

7 Fink, M. Time Reversal of Ultrasonic Fields. I. Basic Principles, *IEEE Transactions on Ultrasonics, Ferroelectrics, and Frequency Control*, 39(5): 555-566, (1992).

8 Aubry, J. F., Tanter, M., Pernot, M., Thomas, J. L., and Fink, M. Experimental Demonstration of Noninvasive Transskull Adaptive Focusing Based on Prior Computed Tomography Scans, *The Journal of the Acoustical Society of America*, 113(1): 84-93, (2003).

9 Mainardi, F. Fractional Calculus and Waves in Linear Viscoelasticity: An Introduction to Mathematical Models, *World Scientific*, (2010).

10 Graves, R. W. Simulating Seismic Wave Propagation in 3D Elastic Media Using Staggered-grid Finite Differences, *Bulletin of the Seismological Society of America*, 86(4): 1091-1106, (1996).

11 Berenger, J. P. A Perfectly Matched Layer for the Absorption of Electromagnetic Waves, *Journal of Computational Physics*, 114(2): 185-200, (1994).

12 Top, C. B., White, P. J., and McDannold, N. J. Nonthermal Ablation of Deep Brain Targets: A Simulation Study on a Large Animal Model, *Medical Physics*, 43(2): 870-882, (2016).